ELSEVIER

Earth and Planetary Science Letters 204 (2002) 363–372

EPSL

www.elsevier.com/locate/epsl

New insights on long distance fault interaction

D. Melini, E. Casarotti, A. Piersanti *, E. Boschi

Istituto Nazionale di Geofisica e Vulcanologia, Via di Vigna Murata 605, I-00143 Rome, Italy

Received 12 June 2002; received in revised form 7 October 2002; accepted 7 October 2002

Abstract

We investigated the plausibility of remote fault triggering on a global scale as a result of postseismic stress transfer by large earthquakes. Previous studies have shown that the postseismic stress field generated by eight of the largest events that have occurred in the Pacific area promoted the rupture of 53.6% of all the $M \geq 5$ events recorded in the last century in the circumpacific ring. We tried to assess the statistical significance of this result by performing a set of new statistical simulations involving very intensive computational tasks. To this aim we implemented a new numerical procedure based on parallel codes. We found that our simulations did not show strong statistical evidence, but there was a clear indication that as we applied more realistic geometrical constraints to the synthetic distributions, we tended to reproduce more closely the observed quantities. These results support the hypothesis of some kind of physical connection of the configuration of a plate margin and its activity with those of all the other plate margins, more than the possibility of remote fault interaction in the 'classical' sense.

Keywords: postseismic stress; viscoelastic relaxation; fault interaction; global scale; synthetic catalogues; supercomputing application

1. Introduction

While fault interaction at a local or regional scale is supported by wide phenomenological evidence and is now considered an important feature in seismic hazard assessment, the possibility of interaction between seismogenic structures at longer distances is still an open question [1,2].

The idea of fault interaction on a global scale was first introduced by Romanowicz [3], who searched for patterns of energy release in the seismic activity of the Pacific area and observed periods of alternating prevalent strike-slip and dip-slip activity at the opposite margins of the Pacific.

Pollitz et al. [4] focused on the sequence of large intraplate earthquakes from 1952 to 1965 along the Aleutian arc and Kurile–Kamchatka trench, pointing out that postseismic stress evolution across the northern Pacific and Arctic basins is consistent with long distance triggering of oceanic intraplate earthquakes.

Casarotti et al. [5] tested the plausibility of fault interaction on a global scale by means of a de-

* Corresponding author. Fax: +39-6-5186-0507.
E-mail address: piersanti@ingv.it (A. Piersanti).

0012-821X/02/$ – see front matter
PII: S0012-821X(02)01006-3

tailed analysis of postseismic stress diffusion in the Pacific area. They assessed the effect of remote stress transfer by calculating the time-dependent global postseismic stress field generated by eight earthquakes, chosen from among the largest ones that occurred in the circumpacific ring during the last century. By evaluating the cumulative stress field induced at the location of each earthquake contained in a subset of the CMT catalogue, Casarotti et al. [5] found a positive induced CFF (Coulomb failure function) variation, which corresponds to a stress field promoting the fault rupture, in 53.6% of the receivers.

In order to assess the statistical significance of this slight excess of facilitated ruptures, Casarotti et al. [5] performed some Monte Carlo simulations. In each simulation they generated a set of 1000 random synthetic catalogues of receiver earthquakes, and for each synthetic catalogue they computed the fraction of receivers with positive ΔCFF associated with the postseismic stress field induced by the eight real events. This was done for three different sets of random synthetic catalogues, each one generated with different statistical properties. The distribution of the fraction of promoted ruptures for each of the three simulations turned out to be almost perfectly normal. The observed fraction of 'triggered' receivers fell, in the worst case, at more than 4 standard deviations from the center of the distribution obtained from the simulation.

These results led Casarotti et al. [5] to the conclusion that the role of postseismic stress transfer at a global scale is not marginal in the assessment of the spatio-temporal pattern of the seismic activity of the Pacific area, and that there must be a physical connection between the postseismic stress field, the geometrical pattern of promoted earthquakes and the distribution of fault plane orientation around the Pacific ring.

In the present work we carried out a new set of simulations which are complementary to the ones performed by Casarotti et al. [5]. In particular, Casarotti et al. were not able to perform any statistical simulations involving the generation of synthetic catalogues of source earthquakes due to excessive computational requests. We have overcome this problem both by implementing a new numerical procedure and by using for our computations a cluster of parallel supercomputers.

In Section 2 we outline the basic features of our numerical procedure, while in Section 3 we present the results of our new simulations and we analyze the connection between regional pattern of seismic moment release and fraction of promoted events.

2. Numerical simulation

2.1. The model and its implementation

The most important tool to assess the interaction between a postseismic residual stress field and a preexisting seismogenic structure is represented by the CFF method [1]. If the six components of the stress tensor and the orientation of the fault plane are known, it is possible to evaluate the variation of the CFF, which is defined as:

$$\Delta\mathrm{CFF} = \Delta\tau + \eta\Delta\sigma$$

where η is a constant depending on the static friction coefficient, the hydrostatic pressure and the pore fluid pressure [1], while σ and τ are the normal and tangential components of the stress field on the seismogenic structure. The knowledge of the CFF variation on a fault tells us if the associated stress field variation is acting to facilitate (positive ΔCFF) or to oppose (negative ΔCFF) the fault rupture.

To compute the CFF on any fault plane in the Pacific area at the time of its rupture we need to know the time evolution of all six components of the stress tensor at the location of each fault and the orientation of the fault planes.

Following [5], we obtained the time evolution of stress tensors using the model of time-dependent viscoelastic postseismic relaxation developed by Piersanti et al. [6,7].

This model is based on a normal mode decomposition of the observable physical quantities in order to solve semi-analytically the equilibrium equation for a spherical, incompressible, self-gravitating Earth subject to a seismic excitation.

The model is laterally homogeneous and includes an 80 km thick elastic lithosphere, a 200 km thick asthenosphere over a uniform mantle characterized by a viscoelastic Maxwell rheology, and a fluid inviscid core. The mantle and asthenospheric viscosity are set to 10^{21} Pa s and 10^{18} Pa s respectively, while the density and shear modulus are obtained by volume-averaging the PREM reference model values.

The numerical solution of the model consists of two distinct steps. First we compute the coefficients of the harmonic expansion of the stress tensor. In this first step the only information we need, beyond the physical parameters of the stratification model, are the depth of the source, the dip and the rake angles, the temporal delay between the source and the solution time, and the depth of the solution. The scalar seismic moment is also needed, but since it affects the stress tensor only by a normalization factor it can be safely set to a standard value (in our case 10^{21} Nm), rescaling the computed stress tensor by the correct factor.

Once the harmonic coefficients are known, the stress tensor at any point on the layer of specified depth can be computed by proper summation of the corresponding spherical harmonic terms. This second step requires knowledge of the remaining parameters, namely the strike angle and the latitude and longitude of the desired point.

The most computationally intensive task is the generation of the harmonic coefficients, because the spherical harmonics summation has a slow convergence, especially when the solution depth is very close to the source depth [8,9], so we need to compute harmonic coefficients up to very high degrees.

To speed up our numerical simulation, we chose a discrete set of values for each parameter on which the harmonic coefficients depend, and built a database of harmonic coefficients corresponding to all the possible (physically meaningful) combinations of the parameters. In the rest of the simulation, when we need to compute the stress tensor for a particular pair of source and receiver events, we chose the pre-computed set of coefficients with parameters that most closely approximate the physical parameters of our source–receiver set and used these coefficients to perform the summation of spherical harmonics. In this way we drastically reduced the CPU time needed for our simulation at the cost of a slight approximation.

The discrete values chosen for harmonic coefficient generation were: 10, 20, ..., 80 km for source and solution depth, 0, 5, 10, ..., 60 yr for source–solution delay and 6, 9, ..., 45° for dip angle.

The rake angle of the source events in our work has been considered fixed to 90°. The motivation of this choice lies in the fact that virtually all extremely large earthquakes are almost purely thrusts, and the ones whose focal mechanism is known have rake angles equal or very close to 90°. On the other hand, the main source of approximations in our numerical computations is the discrete sampling of the other parameters described above, so the assumption of fixed rake angle is within the limits of our precision, but at the same time enables us to drastically reduce the CPU time required by our simulations, which is the crucial limiting factor.

The generation of the coefficient database has been run on a Digital AlphaServer 2100A and took about 24 h of CPU time, producing nearly 50 GB of output data.

2.2. Source and receiver catalogues

Our numerical simulation implied computation of the postseismic stress field induced by each source event contained in a set of randomly generated sources (synthetic catalogue) at the locations of each earthquake in the Pacific area.

The catalogue of receiver events is a subset of the Centroid Moment Tensor (CMT) Project catalogue [10]. The events were selected by first extracting the ones located in the Pacific area (with coordinates ranging from 120° to 300° longitude and from −60° to 80° latitude) with magnitude $M \geq 5$, then running on this subset a semi-automatic fault plane identification procedure, described in detail in [5]. This procedure chose the most reasonable fault plane solution, since to obtain the CFF value we need the fault plane orientation, and discarded the events for which the actual fault plane was not discernible. After these

selections, we obtained a catalogue of 8131 events located in the circumpacific ring, which we will from now on call the 'receiver catalogue'.

It is worth observing that even though the CMT catalogue is not complete for magnitudes greater than or equal to 5.0, this incompleteness will not affect the results of our analysis. Indeed, in order for this to happen, the events missing from the CMT catalogue should have a coherent behavior in the interaction with the postseismic stress field, for instance should be preferentially favored. In this way the resulting fraction of favored ruptures would be affected by the missing events. Since there is no reason to expect such a behavior, we can safely neglect the incompleteness of the CMT catalogue. The same kind of argument holds for the selection effect introduced by the fault plane identification procedure, which removes from the catalogue the events with unresolvable fault planes.

The source catalogues were generated randomly, with different criteria of extraction of the various parameters. First, we generated two source databases, each containing 10^4 synthetic source events. The first database (a) was generated with source locations regionally distributed along the circumpacific ring, and with probability of occurrence proportional to the local density of CMT events. The second database (b) also has sources distributed along the circumpacific ring, but with uniform probability of occurrence. For both databases, the source depth was uniformly chosen from 10 to 80 km, the origin time from 1900 to 2000, the strike angle between 0 and 360° and the dip angle between 6 and 45°. The rake angle, as stated above, was fixed to 90°.

With each source database, we built three different sets of synthetic catalogues by randomly extracting sources from each database according to different selection criteria. In this way, each

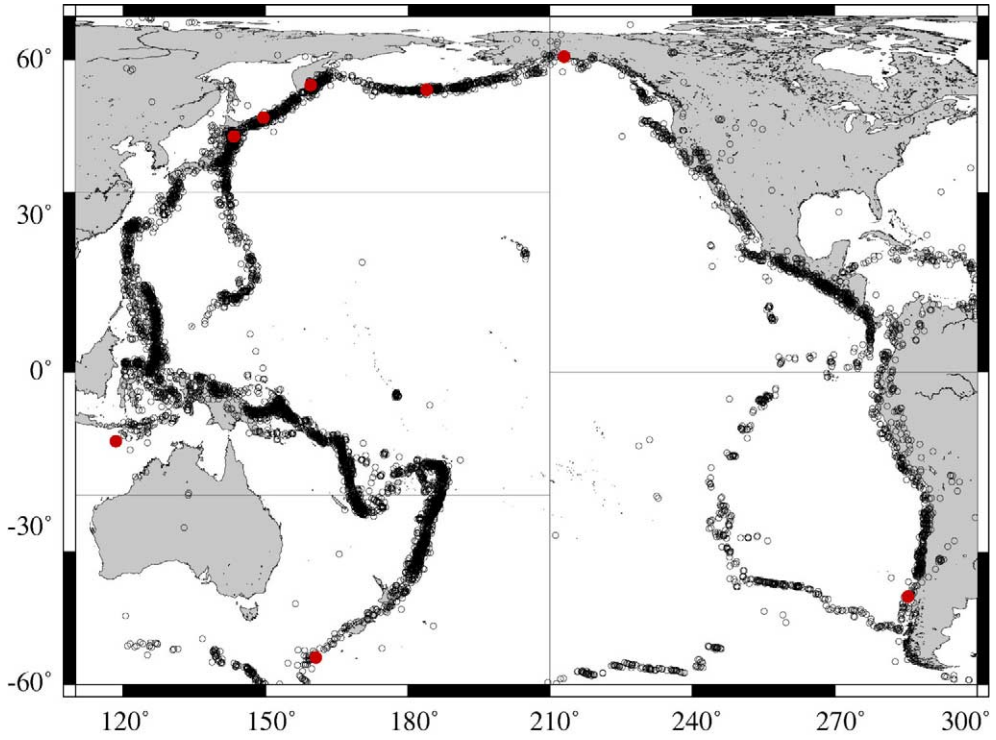

Fig. 1. Geographic distribution of the receiver events. The red circles correspond to the locations of the eight real source events (Chile 1960, Alaska 1964, Kamchatka 1952, Aleutian 1957, South Kurils 1963, Japan 1968, Java 1977 and Maquarie Ridge 1989). The solid lines are the delimitation of the five macroregions defined for the generation of regionally distributed synthetic catalogues.

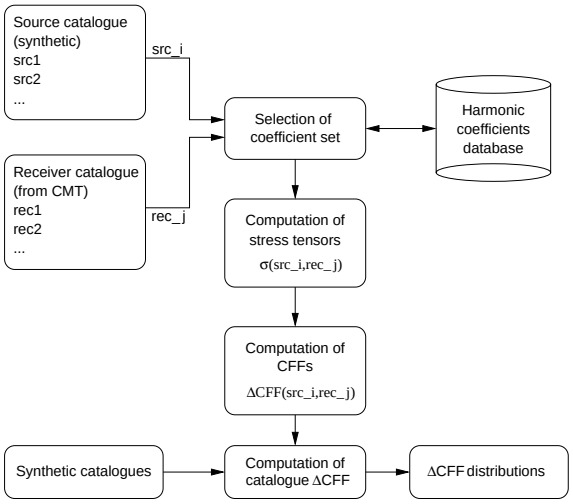

Fig. 2. Block diagram of the simulation. First, a database of harmonic coefficients is computed containing coefficient sets for all the combinations of source and receiver depth = 10, 20, ..., 80 km, source–receiver temporal delay = 0, 5, ..., 60 yr and dip angle = 6, 9, ..., 45°. Then, for each source–receiver pair obtained with sources from a synthetic source database and receivers from the CMT Project catalogue, the set of harmonic coefficients which most closely approximate the physical parameters is selected and is used to compute the stress tensor induced by the source on the location of the receiver. Once all the stress tensors are known, it is possible to compute on each receiver fault plane the ΔCFF corresponding to the postseismic stress field induced by each source. After that, for each set of synthetic catalogues, the overall ΔCFF for each receiver fault plane is derived by summing the eight ΔCFFs corresponding to the eight sources contained in the synthetic catalogue. Finally, for each synthetic catalogue the fraction of 'triggered' receivers (i.e. those with positive ΔCFF) is evaluated. Repeating these last steps for each synthetic catalogue and for various synthetic source databases leads to the ΔCFF distributions shown in Fig. 4.

synthetic catalogue will be characterized both by the criteria used for source extraction and by the statistical properties of the source database from which the events have been extracted.

Each synthetic catalogue consists of eight sources, which reflect the number of 'real' earthquakes used in [5]. Two different criteria were defined to extract the eight synthetic source events which compose a synthetic catalogue: (1) completely random and (2) reproducing the geographic distribution of the real sources. In the latter case we subdivided the Pacific area into five 'macroregions' (see Fig. 1) and, among all the synthetic sources falling into a particular macroregion, we randomly extracted a number of sources equal to the number of real sources falling into the same macroregion. To complete the generation of the synthetic catalogues, we need to assign to each source a seismic moment. We defined two different strategies of seismic moment assignment: (1) assigning the seismic moments of the eight real sources randomly to the synthetic sources and (2) assigning the seismic moments of the real sources falling into a macroregion to the synthetic source extracted from the same macroregion. The second method is applied only to synthetic catalogues with 'regionalized' sources.

Considering all the possible combinations of source selection and seismic moment assignment strategies, we can build three different kinds of synthetic catalogues for each source database, so we have six possible simulations, which are summarized in Table 1.

The main part of our numerical work consists in generating sets of 10^4 synthetic catalogues for each simulation listed in Table 1 and computing

Table 1
Summary of statistical simulations

Simulation number	Source database	Source selection	Seismic moment assignment
1	CMT Local density (a)	Random	Random
2	CMT Local density (a)	Regional	Random
3	CMT Local density (a)	Regional	Regional
4	Uniform density (b)	Random	Random
5	Uniform density (b)	Regional	Random
6	Uniform density (b)	Regional	Regional

the corresponding distribution of the fraction of $\Delta CFF > 0$ receiver events. The process is outlined in Fig. 2. First, we compute the postseismic stress field induced by viscoelastic relaxation by each source event contained in our databases on each receiver fault plane. After that, for each synthetic catalogue we know the contribution of the eight sources contained in the catalogue itself to the stress tensor on each receiver fault plane, so we can compute the corresponding ΔCFF. This procedure implies the application of the viscoelastic relaxation code to over 2×10^8 source–receiver event pairs. The computation was performed on an IBM RS6000/SP2 parallel machine and took about 500 h of CPU time using an OpenMP parallel code running on 10 processors.

3. Results and discussion

3.1. Statistical analysis

In Fig. 3 we plot the distribution of fractions of $\Delta CFF > 0$ events obtained in each simulation. As in [5], the distributions were almost perfectly normal. In Fig. 4 we report for each simulation the mean value and the standard deviation of the distribution, as obtained by fitting the histograms with a normal curve.

Even though all our simulations always give a fraction of $\Delta CFF > 0$ events lower than the observed value, which is in the same direction as the results of Casarotti et al. [5], our results do not provide strong statistical significance, the ob-

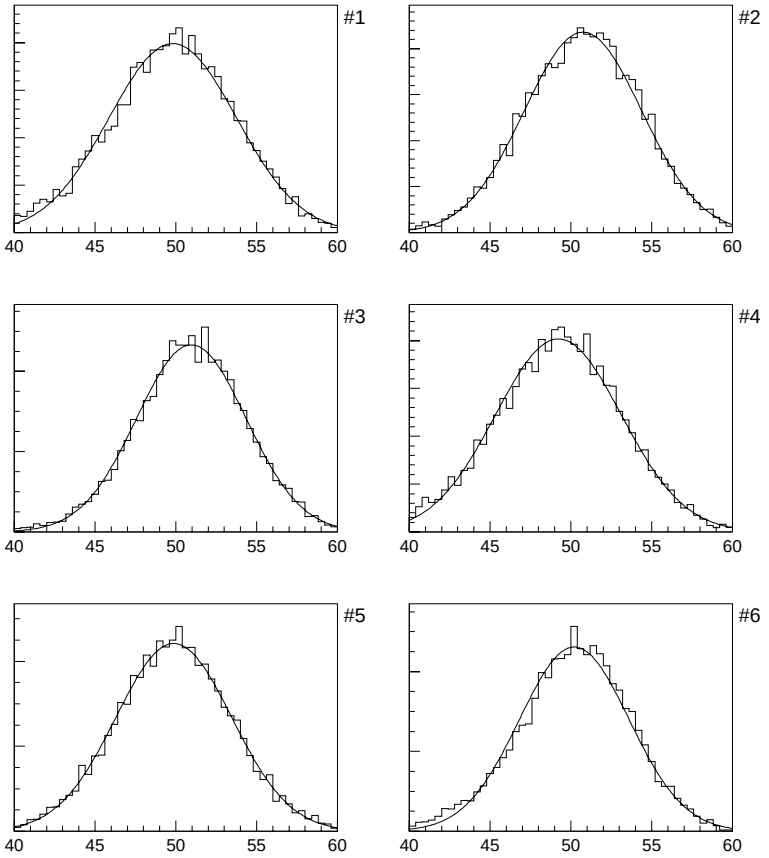

Fig. 3. Distribution of the fraction of events with $\Delta CFF > 0$ for the six simulations listed in Table 1.

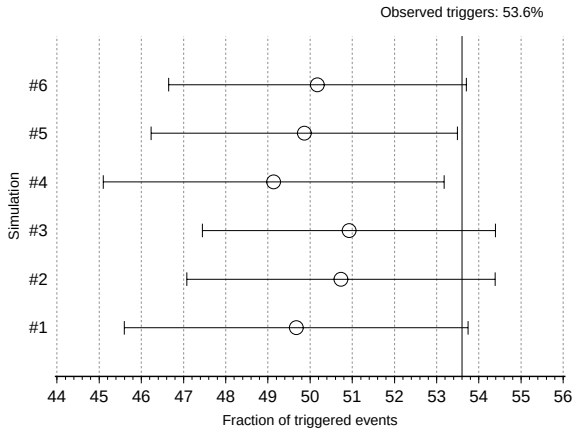

Fig. 4. Mean value and standard deviation of the distribution of fractions of $\Delta CFF > 0$ events ('triggered events') for the simulations listed in Table 1. The solid line represents the fraction of $\Delta CFF > 0$ events found in the real case, as derived in [5].

served fraction of promoted events being at a distance always near to one standard deviation from the center of the distribution.

Nevertheless, we can see from Fig. 4 that simulations 1, 2 and 3 reproduce more closely the observed value than the other three simulations. Simulations 1, 2 and 3 are built with random synthetic catalogues with event probability proportional to the local density of CMT events; this may be an indication of the fact that when we apply realistic physical constraints to our random sources, the result of the simulation approaches more closely the observed value.

In any case we stress again that, from a quantitative point of view, all the results of our simulations are compatible with the observed fraction of promoted events, so we cannot exclude at this level that the slight excess of promoted ruptures observed by Casarotti et al. [5] was observed by chance.

3.2. *Analysis of spatial distribution of seismic moment*

In the following, we investigate the features of the spatial distribution of seismic moment released by synthetic catalogues which reproduce most closely the observed case.

We considered simulations 1 and 4, i.e. those with random selection of synthetic sources and random assignment of seismic moment. For both simulations, we subdivided the 10^4 synthetic source catalogues into 10 bins. The first bin contains the synthetic source catalogues which give a fraction f_+ of promoted ruptures between 40% and 42%; the second bin contains the synthetic catalogues which give f_+ between 42% and 44%, and so on until the 10th bin which contains catalogues giving $58\% < f_+ \leq 60\%$.

For each bin, we plotted on a map the mean seismic moment release of all the synthetic source catalogues belonging to that bin. The maps relative to simulations 1 and 4 are given in Figs. 5 and 6 respectively.

In both figures we can see a smooth change of the pattern of seismic moment release as we move from the first (Figs. 5a and 6a) to the last bin (Figs. 5j and 6j). We can also note that the synthetic catalogues with a spatial distribution of released seismic moment closest to the real pattern of seismic moment release (Figs. 5g,h and 6g,h) are the ones which also give a fraction of promoted ruptures in the receiver catalogue very close to the observed 53.6%.

The importance of these results lies in the fact that the synthetic catalogues used in the chosen simulations are built by selecting groups of eight sources in a completely random way among the sources contained in each database. In this way there is no biasing effect in the synthetic catalogue except the statistical properties of the synthetic sources. So, it appears to be remarkable that among all the possible random groups of eight synthetic sources that we can generate, only the ones that happen to give f_+ near to 53.6% are also the ones that give a pattern of energy release which is the most similar to the physical one. These results may suggest the hypothesis of plate margin configuration as a self-organized system on a global scale.

4. Conclusions

From our analysis we can draw two main conclusions. Differently from the simulations involv-

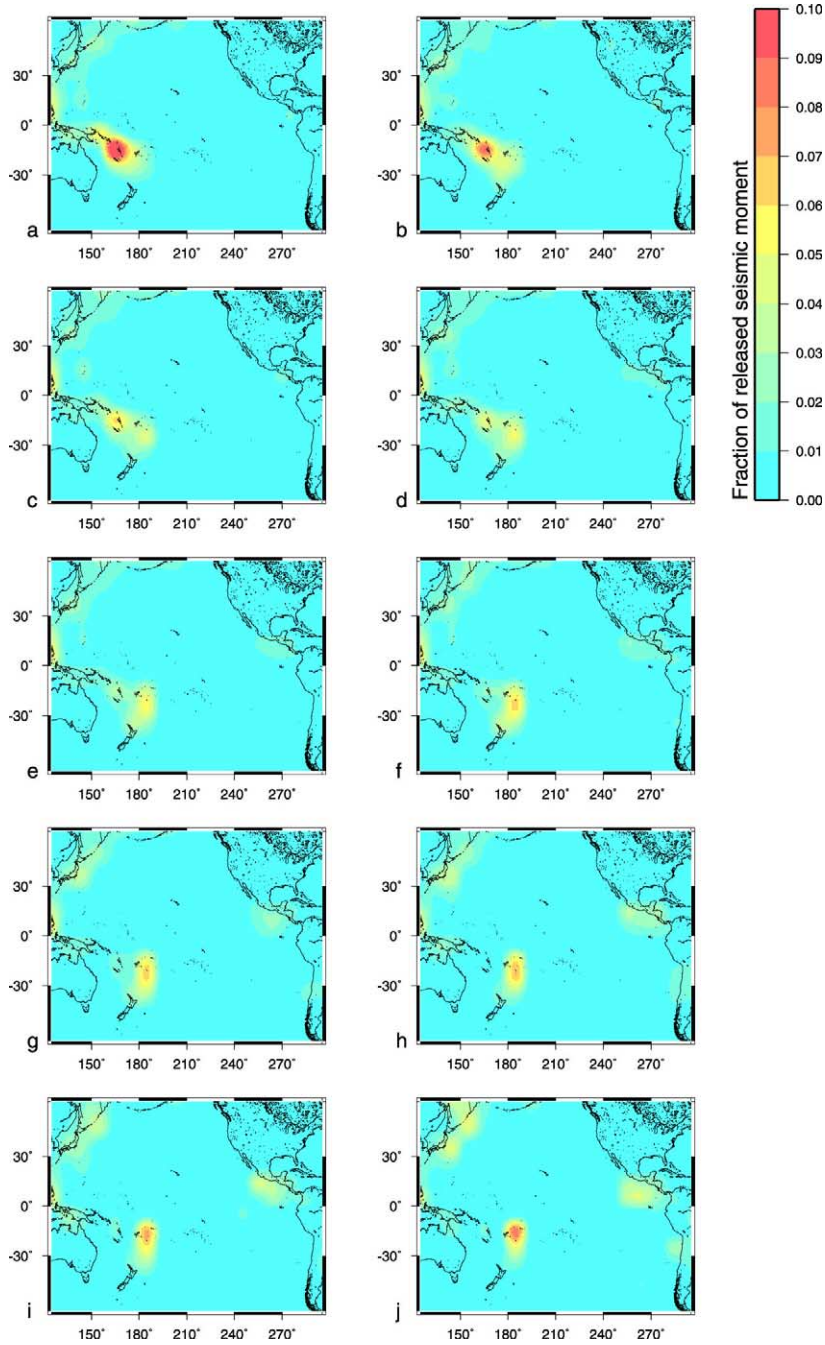

Fig. 5. Maps of seismic moment release for random synthetic catalogues based on the database of synthetic sources with event probability proportional to the local CMT event density (simulation 1). Each panel shows the geographical distribution of mean seismic moment release over all the synthetic catalogues which generate a fraction f_+ of $\Delta CFF > 0$ receiver events contained in the corresponding bin. The bins are defined as follows: $40\% < f_+ \leq 42\%$ (panel a), $42\% < f_+ \leq 44\%$ (panel b), $44\% < f_+ \leq 46\%$ (panel c), and so on until $58\% < f_+ \leq 60\%$ (panel j).

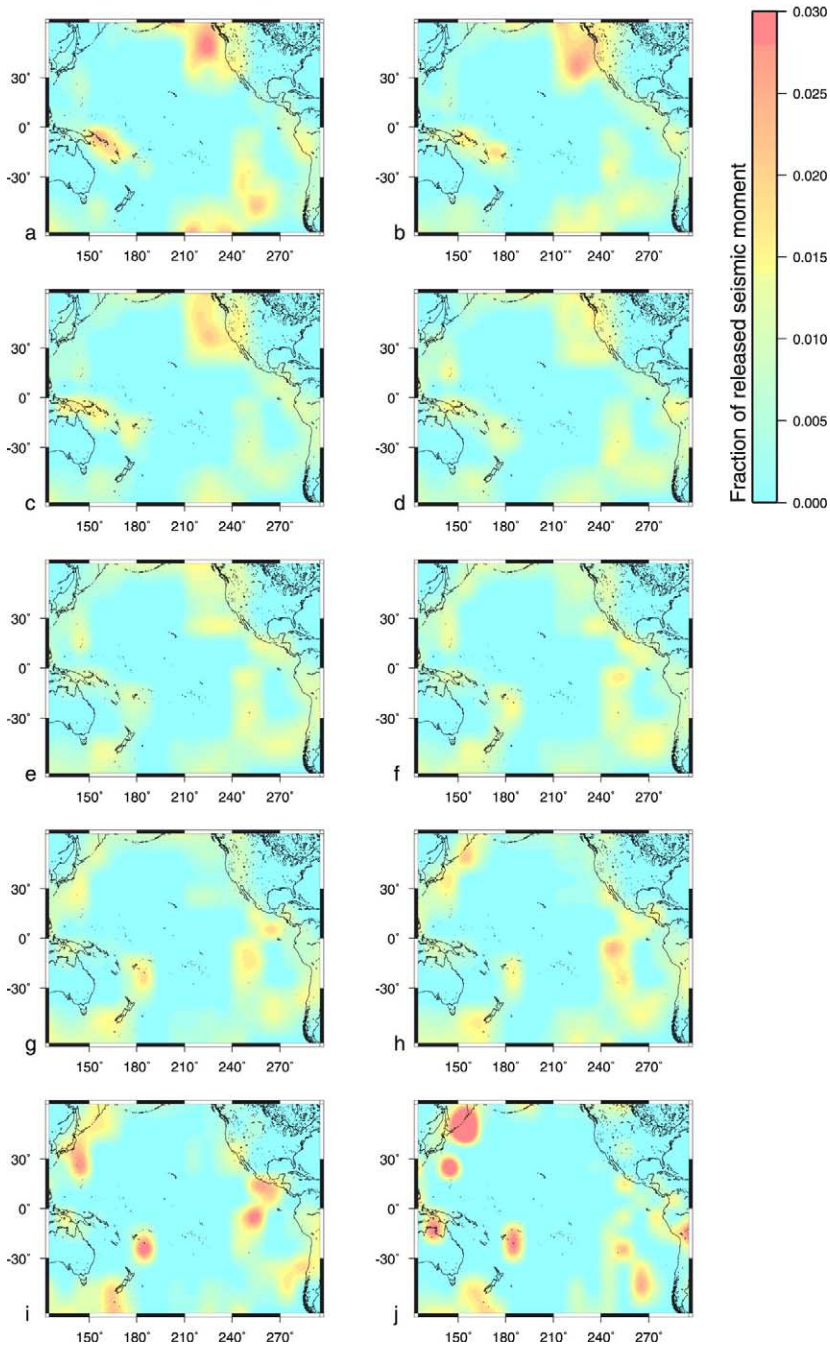

Fig. 6. Maps of seismic moment release as in Fig. 5 for random synthetic catalogues based on the database of synthetic sources with uniform event probability (simulation 4).

ing synthetic distributions of receiver earthquakes [5], simulations obtained using synthetic distributions of source earthquakes (which is the new feature of the present work) do not give significant statistical evidence, even though the simulations give a fraction of $\Delta CFF > 0$ receiver events lower than the observed one, which is in the same direction as the results obtained by Casarotti et al. [5].

On the other hand, examining in depth the simulation results, we see that the synthetic distributions with more realistic geometrical properties tend to reproduce closely the observed fraction of $\Delta CFF > 0$ receiver events. This is evidence supporting the hypothesis proposed on a speculative basis by Casarotti et al. [5], which pointed out that the statistical irregularities observed in the $\Delta CFF > 0$ event distributions might be concerned with the geometrical plate margin configuration, more than a remote fault triggering effect in the 'classical' sense.

This, far from definitely closing the problem, opens new interesting interpretative frameworks. Indeed, there is no obvious a priori explanation for why the global geometrical configuration of the plate margins and the global mechanism of seismic energy release should be connected. The crucial point in this context is represented by the word 'global': in fact, the existence of a physical connection between the configuration of a single plate margin and the seismic activity in that margin could be considered trivial, but surely the possibility that our results suggest, of a physical connection between the configuration of a plate margin and its activity with the configuration of all the other plate margins and their seismic activity, is not trivial.

Acknowledgements

We thank F.P. Lucente for the fruitful collaboration in developing the CMT fault plane identification procedure.*[AC]*

References

[1] R.S. Stein, The role of stress transfer in earthquake occurrence, Nature 402 (1999) 605–609.
[2] R.A. Kerr, Can great earthquakes extend their reach?, Science 280 (1998) 1194–1195.
[3] B. Romanowicz, Spatiotemporal patterns in the energy release of great earthquakes, Science 260 (1993) 1923–1926.
[4] F.F. Pollitz, R. Bürgmann, B. Romanowicz, Viscosity of oceanic astenosphere inferred from remote triggering of earthquakes, Science 280 (1998) 1245–1249.
[5] E. Casarotti, A. Piersanti, F.P. Lucente, E. Boschi, Global postseismic stress diffusion and fault interaction at long distances, Earth Planet. Sci. Lett. 191 (2001) 75–84.
[6] A. Piersanti, G. Spada, R. Sabadini, Global postseismic rebound of a viscoelastic Earth: Theory for finite faults and application to the 1964 Alaska earthquake, J. Geophys. Res. 102 (1997) 477–492.
[7] A. Piersanti, G. Spada, R. Sabadini, M. Bonafede, Global postseismic deformation, Geophys. J. Int. 120 (1995) 544–566.
[8] C. Nostro, A. Piersanti, A. Antonioli, G. Spada, Spherical versus flat models of coseismic and postseismic deformations, J. Geophys. Res. 104 (1999) 115–134.
[9] W. Sun, S. Okubo, Surface potential and gravity changes due to internal dislocations in a spherical Earth; I, Theory for a point dislocation, Geophys. J. Int. 114 (1993) 569–592.
[10] A.M. Dziewonski, G. Ekstrom, N. Maternovskaya, R. Abercrombie, M. Antolik, M. Nettles, Centroid Moment Tensor Project, http://www.seismology.harvard.edu/projects/CMT/, 2000.